JOURNAL OF PROPULSION AND POWER
Vol. 24, No. 2, March–April 2008

Heating and Ignition of Metallic Particles by a CO_2 Laser

Salil Mohan,* Mikhaylo A. Trunov,† and Edward L. Dreizin‡
New Jersey Institute of Technology, Newark, New Jersey 07102

DOI: 10.2514/1.30195

This paper presents an experimental technique and respective heat transfer model for studying ignition of micron-sized metallic particles at varied heating rates in the range of 10^6 K/s. The experimental setup uses a CO_2 laser as a heating source. The interaction of the laser beam with particles is particle size dependent and a narrow range of particle sizes (around 3.37 μm) is heated most effectively. Therefore, the heat transfer model needs to be analyzed only for the particles with this specific size, which greatly simplifies the interpretation of experiments. The powder is aerosolized inside a plate capacitor by charging particles contacting the capacitor's electrodes. A thin, laminar aerosol jet is carried out by an oxidizing gas through a small opening in the top electrode and is fed into a laser beam. The velocities of particles in the jet are in the range of 0.1–3 m/s. For each selected jet velocity, the laser power is increased until the particles are observed to ignite. The ignition is detected optically using a digital camera and a photomultiplier. The ignition thresholds for spherical aluminum powder were measured at three different particle jet velocities resulting in three different heating rates. The experimental data for aluminum, for which the ignition kinetics parameters are known, were acquired at a specific heating rate and used to calibrate the detailed heat transfer model. The experiments with different heating rates were performed to validate the model. The developed experimental technique and the heat transfer model can now be used to determine the ignition kinetics of different metallic powders in various gas environments.

Nomenclature

A	=	accommodation coefficient
C	=	particle specific heat, $J \cdot kg^{-1}$
D	=	particle diameter, m
D_{beam}	=	laser beam diameter, m
f	=	particle complex refractive index
I	=	laser beam intensity, $J \cdot m^{-2} \cdot s^{-1}$
i	=	power law coefficient for gas thermal conductivity
K_B	=	Boltzmann constant, $J \cdot K^{-1}$
k_g	=	gas thermal conductivity, $J \cdot m^{-1} \cdot s^{-1} \cdot K^{-1}$
M	=	particle mass, kg
m_g	=	mass of gas molecule, kg
P_g	=	ambient gas pressure, $N \cdot m^{-2}$
$\dot{Q}_{Chemical}$	=	chemical heat generation rate, $J \cdot s^{-1}$
$\dot{Q}_{Convection}$	=	convection heat transfer rate, $J \cdot s^{-1}$
$\dot{Q}_{Laser}$	=	laser heat transfer rate, $J \cdot s^{-1}$
$\dot{Q}_{Radiation}$	=	radiation heat transfer rate, $J \cdot s^{-1}$
$\dot{q}_{Continuum}$	=	continuum heat transfer rate, $J \cdot s^{-1}$
$\dot{q}_{Free\ molecular}$	=	free-molecular heat transfer rate, $J \cdot s^{-1}$
T_g	=	ambient gas temperature, K
T_p	=	particle temperature, K
T_δ	=	gas temperature at Langmuir layer, K
t	=	time, s
W	=	total laser beam power, $J \cdot s^{-1}$
z	=	coordinate perpendicular to laser beam axis, m
α	=	particle's thermal diffusivity, $m^2 \cdot s^{-1}$
γ	=	adiabatic index of gas
γ^*	=	adiabatic index of gas, averaged over T_p and T_δ
δ	=	Langmuir layer thickness, m
ε	=	particle emissivity
η	=	particle's laser absorption efficiency
λ	=	CO_2 laser wavelength, m
λ_{MFP}	=	mean free path of monoatomic gas molecule, m
λ'_{MFP}	=	mean free path of polyatomic gas molecule, m
σ	=	Gaussian standard deviation, m
σ_{SB}	=	Stefan–Boltzmann constant, $J \cdot m^{-2} \cdot s^{-1} \cdot K^{-4}$
τ	=	particle temperature equilibration time, s

Presented as Paper 1428 at the 45th AIAA Aerospace Sciences Meeting and Exhibit, Reno, Nevada, 8–11 January 2007; received 1 February 2007; accepted for publication 2 September 2007.

*Graduate Research Assistant, Department of Mechanical Engineering. Student Member AIAA.
†Research Scientist, Department of Chemical Engineering.
‡Professor, Department of Chemical Engineering. Senior Member AIAA.

I. Introduction

REACTIVE metals and metalloids, for example, Al, B, Mg, Zr, Ti, Li, etc., as well as their alloys are promising ingredients for high-energy density compositions used in propulsion systems, explosives, and pyrotechnics. Metallic powder fuel additives enable one to achieve higher combustion enthalpies and reaction temperatures. In most practical systems, metal ignition and combustion occur in environments with rapidly changing temperatures and gas compositions. On the other hand, most of the available quantitative characteristics describing ignition and combustion of metal particles were obtained from laboratory experiments in which the environment temperature and composition were carefully controlled. Thus, ignition of metallic particles has been often characterized by a predetermined ignition temperature [1,2]. Ignition is also commonly assumed to occur after an ignition delay, which is estimated as the time required to preheat the particle up to the ignition temperature. The ignition temperature is classically understood in terms of Semenov's thermal theory as the minimum environment temperature which leads to self-sustaining combustion of an inserted particle [3,4]. This definition has been successfully used for applications where the heating rates are characteristically low, for example, dealing with fire safety and ignition of solid fuels in large furnaces [5,6]. However, it becomes inadequate for applications in which the particles are heated rapidly, and the particle's temperature can exceed the classically defined ignition temperature before the self-sustaining combustion is established. Furthermore, the whole concept of ignition temperature appears inadequate considering the nature of heterogeneous oxidation leading to ignition of most metals. For example, for aluminum, the thermally accelerated heterogeneous oxidation producing the heat necessary for a self-sustaining combustion also accelerates the growth of a protective oxide layer,

which could prevent the combustion from occurring. This situation is typical for metal particle ignition in explosives, propellants, and pyrotechnics. Thus, to describe ignition for such applications, it is necessary to analyze the specific transient heat transfer problem in which one or more of the exothermic processes leading to the particle ignition are considered. Such analyses require quantitative descriptions of these, typically thermally controlled, exothermic processes balanced by the conventional heat transfer terms of convection and radiation. The kinetics of exothermic reactions in related energetic materials is commonly characterized by thermal analysis, where the heating rates are very low, on the order of 1–50 K/ min. The extrapolation of the identified kinetics to the high heating rates is difficult and requires direct experimental verification. This difficulty led to the development of new experimental approaches to directly characterize ignition kinetics for the heating rates in the range of 10^3–10^4 K/s [7,8]. However, the practically interesting heating rates of 10^6 K/s range have not been achieved. Also, there is a critical difficulty in the interpretation of all the experimental data dealing with ignition of metal powders, which is caused by the presence of particles of different sizes. The heating rates are different for particles of different sizes, and so must be the rates of the thermally controlled processes leading to ignition. Therefore, interpretation of the experimental data obtained with regular, polydispersed metal powders is difficult, whereas experiments with highly monodispersed particles are impractical.

This study presents a new experimental technique and the corresponding heat transfer model that enables one to quantify ignition kinetics for reactive particles heated at varied heating rates approaching to or exceeding 10^6 K/s. Therefore, the identified ignition kinetics must be directly useful in modeling ignition of such particles in practical applications involving rapid heating. The proposed experimental technique uses CO_2 laser heating of aerosolized powders, which is particle size sensitive. As a result, only particles in a narrow range of sizes are effectively heated and ignited. This allows interpreting the results using a detailed heat transfer model for the specific, effectively heated particle size, even though a commonly available polydispersed powder is used in experiments. The laser is fired at a minimum possible power at which ignition starts to be observed, so that only the most effectively heated particles are ignited. The technique allows achieving different particle heating rates by varying the speed of particles fed into the laser beam. This paper describes the developed experimental technique, the heat transfer model, and experiments aimed to calibrate the model using a metal powder with well-established ignition kinetics.

II. Technical Approach

The technical approach is based on feeding individual micron-sized metal particles into a focused CO_2 laser beam. Because the CO_2 laser wavelength (10.6 μm) is comparable to the particle diameter, the laser heating is particle size dependent and is most effective for the particles of about 3.4 μm in diameter (as discussed in detail later). The experiment is conducted in an oxidizing environment, so that if the laser power exceeds a specific threshold, the heated particles of 3.4 μm diameter start igniting when they cross the laser beam. A detailed heat transfer model is developed, taking into account heating of metal particles in the laser beam, thermally controlled heterogeneous exothermic reactions leading to ignition, convection, and radiation terms. The model needs to consider only the specified above particle diameter, whereas experiments are conducted with a commercial polydispersed Al powder. The model includes one adjustable parameter that is the effective diameter of the focused laser beam. Specifically, it is the standard deviation for the Gaussian function describing the energy distribution across the laser beam. Note that an accurate measurement of the focused CO_2 laser beam diameter is difficult because of the thermal interaction of the beam and any target placed in its focal point. In addition, interference effects become substantial and contribute to the experimental error. Instead, an experimentally determined laser power ignition threshold obtained for spherical Al particles, for which the kinetics of exothermic reactions leading to ignition has been recently described, [9–12] is used to determine the adjustable parameter and thus to calibrate the model. The calibrated model is validated by experiments conducted with the same particles but at different heating rates. The validated model can be used to determine ignition kinetics of different materials igniting in various environments.

III. Experimental

The powder used in these experiments was spherical, 99% pure aluminum with a nominal average particle size of 4.5–7 μm by Alfa Aesar. The experimental setup is shown in Fig. 1 and includes a generator of an aerosol jet, a 125 W CO_2 laser (Synrad, Evolution 125) with a ZnSe convex lens (0.75 in. aperture and 4 in. focal length), and a modulated green laser (SUWTECH model DPGL-3000 by Photop Technologies, Inc.) operated with a set of a semicylindrical and convex glass lenses to produce a laser sheet for the jet visualization. Also, not shown in Fig. 1 but employed in the experiments were a digital camera (Panasonic GS-35), used to obtain particle streaks, and a photomultiplier tube (PMT) used to identify events of particle ignition. In addition, a power meter (Synrad, POWER WIZARD 250), was used to measure the laser beam energy and verify the accuracy of the preset laser power.

The aerosol jet generator uses electrostatic aerosolization described elsewhere [13]. In this technique, a conductive (e.g., metal) powder is placed between the electrodes of a parallel plate capacitor. A high dc voltage in the range of 1–15 kV is applied and conductive particles acquire electric charge. They are repelled from the bottom electrode and attracted to the top electrode, where they recharge upon collision. The motion of the charging and recharging particles continues so that an aerosol is produced in the space between the capacitor's electrodes. Because of the multiple collisions of the charged particles with electrodes, particle agglomerates are broken and the resulting jet contains single particles only, as was confirmed in the previous reports [14]. The applied voltage can be used to control the particle number density in the produced aerosol. In the device used in this project, a small opening (nozzle) was made in the center of the top electrode to allow formation of a thin aerosol jet escaping from the capacitor. The number density of the produced aerosol was maintained small so that the number of particles fed into the aerosol jet was of the order of 1000 per second. The space between the capacitor's electrodes was enclosed in a chamber. A controlled airflow, measured by a gas flow meter (M-200SCCM-D by Alicat Scientific, Inc.), was fed into the chamber to adjust the speed of the escaping laminar aerosol jet. The speed could be readily controlled in the range of 0.1–3 m/s. An additional, slow (~0.1 m/s) shroud airflow (not shown in Fig. 1) was also produced around the aerosol jet, which was found to enhance the jet's stability [13].

The aerosol jet was illuminated by a vertical green laser sheet. To enable particle image velocimetry, the laser sheet was modulated at 600, 1500, and 2000 Hz, depending on the jet speed. Produced particle streaks were recorded using the digital camera and the streak lengths were measured to determine the jet velocity.

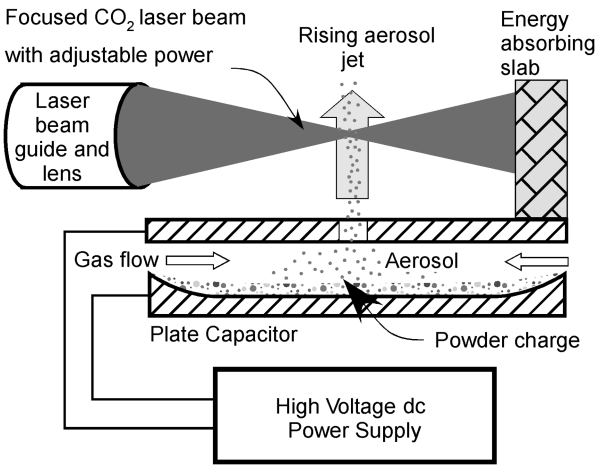

Fig. 1 Schematic diagram of the experimental setup.

The CO_2 laser was focused about 1.5 cm above the jet nozzle using an auxiliary red laser aligned with the CO_2 laser beam and the ZnSe lens. Once a stable aerosol jet was established, the CO_2 laser was fired continuously for 8 s, at a preset power level. The visible radiation, generated by heating and/or ignition of particles, was monitored using a photomultiplier connected to a PC-based data acquisition system. The streaks of heated particles were also visualized by a digital camera operated with a shutter open for the entire duration of the laser firing. The experiment was repeated with gradually increased laser powers until ignition was clearly observed. The peaks recorded by the PMT were analyzed to determine the minimum laser power needed for ignition for each specific aerosol jet velocity.

The images recorded by the digital camera showed short and bright streaks of particles crossing the laser beam. However, discrimination between the streaks produced by luminous particles that did not ignite and those that ignited and burned was ambiguous. Thus, using the PMT with a temporal resolution of 20 μs was necessary for clear identification of the ignition events. Typical examples of PMT peaks produced by different particles crossing the laser beam are shown in Fig. 2. Figure 2a shows a peak produced by a particle that ignited and burned. A sharp voltage rise is followed by small changes in the radiation signal occurring during the particle combustion. On the other hand, the peak shown in Fig. 2b shows the heating and cooling of the particle that never ignited, and the voltage rise is immediately followed by the voltage decrease as the particle exits from the beam. The minimum ignition threshold was determined if at least one ignition event was detected during the 8-s period the laser was fired. An 8-s experiment was performed at least 3 times for each laser power setting.

The experiment was performed for three different particle velocities, so that the igniting particles were heated at three different rates. Both the jet velocity and the laser power measurements were repeated immediately before and after each ignition experiment.

In a separate measurement, the effective diameter of the focused laser beam was evaluated. Because the laser energy is distributed across the beam according to a Gaussian profile [15], the laser beam diameter is poorly defined. However, experimentally this diameter was roughly assessed by firing the laser on a ceramic surface and measuring the diameter of the produced impression.

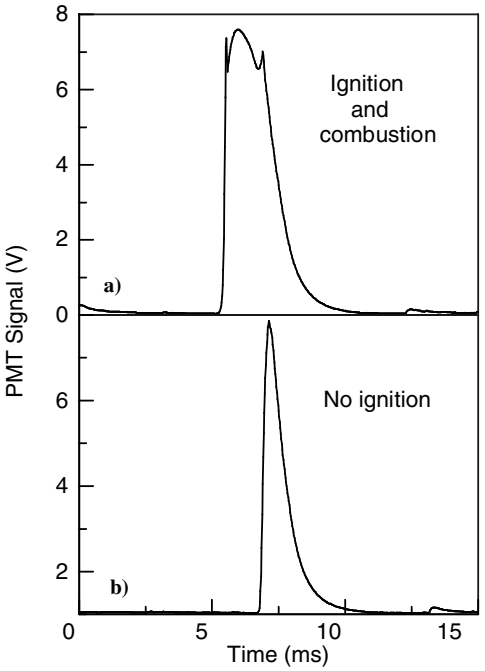

Fig. 2 PMT signal from micron size Al particles crossing the CO_2 laser beam. The aerosol jet velocity is 2.4 m/s and the laser power is 37.7 W. a) Signal corresponding to ignition and combustion of a particle; b) signal corresponding to heating and cooling of an unignited particle.

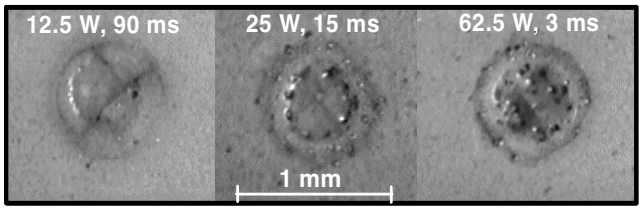

Fig. 3 CO_2 laser beam impressions on a ceramic plate obtained at different laser power levels. The impressions are painted over with a dark marker to improve contrast. The laser powers and exposure times are shown for each impression.

Figure 3 shows magnified images of the impressions obtained at 12.5, 25, and 62.5-W laser powers with exposure time of 90, 15, and 3 ms, respectively. Minimum exposure times required to obtain an impression were used for each laser power setting. The sizes of the external and internal circles observed on the obtained impressions did not change as a function of the laser power and could indicate the diameters of the zone of thermal influence and of the laser beam, respectively. The diameter of the inner circle was measured to be close to 330 μm. This size was considered as an initial approximation for the beam diameter. As described below, the width of the Gaussian distribution of the laser beam energy profile was used as an adjustable parameter in the developed heat transfer model. The measurement using the laser beam impressions served as a guide for the reasonable range, in which the adjustable parameter could vary.

IV. Heat Transfer Model

The model calculates the temperature history of a single particle heated by a focused CO_2 laser beam. The experimental aerosol jet is assumed to be sufficiently thin to neglect the interaction between the particles. For the average feed rate of 1000 particles per second, the particles moving at about 1 m/s were separated from one another by a distance of the order of 1 mm. Because only a fraction of particles was heated by the laser and ignited, the heat transfer between the particles could safely be neglected. If a series of close or overlapping peaks was observed in the PMT traces, such as shown in Fig. 2, such peaks were disregarded.

The particles are heated while crossing the laser beam, so that the characteristic particle heating times, determined by the particle speed and the beam diameter, are in the range of 0.1–3 ms. These times are much longer than the characteristic time of temperature equilibration within the particle, $\tau \approx D^2/\alpha \sim 0.1$ μs, where D is the particle diameter and α is the metal's thermal diffusivity. Thus, the temperature gradients within metal particles are neglected. The model considers only the particles of a selected diameter that are heated by the CO_2 laser most effectively. This diameter is determined below while analyzing the interaction of the laser irradiation with the metal particle.

The particle's temperature history is calculated using the heat balance:

$$MC\frac{\partial T_p}{\partial t} = \dot{Q}_{\text{Laser}} + \dot{Q}_{\text{Chemical}} - \dot{Q}_{\text{Radiation}} - \dot{Q}_{\text{Convection}} \qquad (1)$$

where M is the particle mass, C is its specific heat, and T_p is its temperature; $\dot{Q}_{\text{Laser}}$ is the heat transfer rate to the particle from the laser beam, $\dot{Q}_{\text{Chemical}}$ is the chemical heat generation rate, which is the term describing an exothermic process responsible for ignition, and $\dot{Q}_{\text{Radiation}}$ and $\dot{Q}_{\text{Convection}}$ are the radiation and convection heat transfer rates, respectively. The overall goal of the proposed experimental methodology and this model is to determine the term $\dot{Q}_{\text{Chemical}}$ as a function of temperature, and thus obtain the quantitative description of the ignition kinetics. Therefore, all the other heat transfer terms must be readily calculated. The radiation term is readily determined from the Stefan–Boltzmann law:

$$\dot{Q}_{\text{Radiation}} = \varepsilon\sigma_{\text{SB}}(\pi D^2)\left(T_p^4 - T_g^4\right) \qquad (2)$$

where ε is emissivity, σ_{SB} is the Stefan–Boltzmann constant, T_p and T_g are the particle and ambient air temperatures, respectively, and D is the particle diameter. The value for emissivity was selected based on the literature references [16] for aluminum surface. Note that unless specifically processed, the aluminum surface is always oxidized, similar to the particles addressed in these experiments, validating this selection. The calculation of terms $\dot{Q}_{\text{Convection}}$ and $\dot{Q}_{\text{Laser}}$ is less straightforward. The convection term was calculated considering that for micron-sized particles, the mean free path of the gas molecules is comparable to the particle diameter. As a result, a transition regime heat transfer model based on Fuchs' model [17–20] was used. The laser absorption efficiency of the particle was estimated taking into account the absorption and scattering of the laser beam, due to the comparable particle size and laser wavelength [21–23]. A theoretical analysis describing the laser heating of micron-sized metal particles was reported in the literature [21]. However, the effects of particle melting and the specific distribution of the laser power across the beam have not been considered. The analysis presented in [21–23] was reproduced and expanded in this paper. The width of the laser beam was difficult to determine and it was treated as an adjustable parameter. In order to find this parameter, in these experiments aluminum particles igniting in air were used, for which the ignition kinetics relations were reported recently [9–12]. Therefore, the term $\dot{Q}_{\text{Chemical}}$ was known so that the comparison of the laser power ignition threshold predicted by the model and experimental results was used to fully define the laser heat input to the particle. The developed model and the fully quantified term $\dot{Q}_{\text{Laser}}$ can be used to determine unknown $\dot{Q}_{\text{Chemical}}$ terms for different powders ignited in different environments.

A. Convection Term

For a 3.4-μm diam particle in an atmospheric pressure air at room temperature, the value of the Knudsen number (Kn) is close to 0.03. The conventional, continuum convection model is only valid for $Kn < 0.01$, and at greater values of the Knudsen number, a transition model needs to be considered. The correction for the dimensionless heat transfer coefficient or Nusselt number (Nu) is shown in Fig. 4 for a specific combination of the particle and gas temperatures as relevant to this work. It is clear that the correction is significant compared to $Nu \approx 2$ for continuum heat transfer. Recently, detailed Monte Carlo simulations [17,18] validated a simplified heat transfer model proposed by Fuchs [19,20] for transition heat transfer regime. In the Fuchs's model, a particle is assumed to be surrounded by a hypothetical Langmuir layer with thickness δ. The thickness of this layer is very close to the molecular mean free path in the ambient gas, λ_{MEP}, calculated in [17] as

$$\delta \approx \lambda_{\text{MFP}} = \frac{4}{5}\frac{k_g(T_g)T_g}{P_g}\sqrt{\frac{m_g}{2K_BT_g}} \tag{3}$$

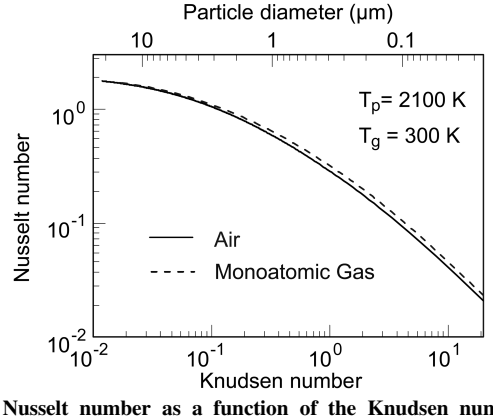

Fig. 4 Nusselt number as a function of the Knudsen number (or particle diameter) is calculated for the transition regime heat transfer using Fuchs's two layer model [17]. Calculations for monoatomic gas are reproduced and the model is adapted for dry air.

where k_g is the gas thermal conductivity, P_g is the gas pressure, m_g is the mass of the gas molecule, and K_B is the Boltzmann constant. Heat transfer within the Langmuir layer is calculated using a free-molecular expression:

$$\dot{q} = \dot{q}_{\text{Free molecular}} = A\pi D^2 P_g \sqrt{\frac{k_B T_\delta}{8\pi m_g}}\frac{\gamma^* + 1}{\gamma^* - 1}\left(\frac{T_p}{T_\delta} - 1\right) \tag{4}$$

where A is the accommodation coefficient, T_δ is the temperature at the boundary of the Langmuir layer, and γ is the adiabatic index of the gas. The superscript * indicates that the value of γ is averaged over the temperature range of $(T_p - T_\delta)$, as described in [17].

Outside the Langmuir layer, the heat transfer is calculated using a continuum regime heat transfer expression:

$$\dot{q} = \dot{q}_{\text{Continuum}} = \frac{4\pi(\delta + D/2)k_g(T_g)T_g}{i+1}\left[\left(\frac{T_\delta}{T_g}\right)^{i+1} - 1\right] \tag{5}$$

where i is the power law dependence coefficient for the gas thermal conductivity (taken as $1/2$ for a monoatomic gas). For a quasi-steady temperature profile, that can be used in this case, Eqs. (4) and (5) are solved iteratively for the temperature at the boundary of the Langmuir layer, T_δ. Once the boundary temperature is found, the rate of heat transfer from the particle to gas is calculated.

The Fuchs's model validated in [17] considered a monoatomic gas and a definition of the mean free path given by Eq. (3). A more generic definition for the mean free path, suitable for polyatomic gases, is commonly considered, for example, [18]:

$$\lambda'_{\text{MFP}} = \frac{4k_g(T_g)}{[9\gamma(T_g) - 5]P_g}[\gamma(T_g) - 1]\sqrt{\frac{\pi m_g T_g}{2k_B}} \tag{6}$$

To use Fuchs's model validated in [17] to describe heat transfer in a polyatomic gas, Eq. (6) should replace Eq. (3) while being corrected by a factor of $3/\sqrt{\pi}$, which is the difference between the two expressions when applied to a monoatomic gas. Thus, the corrected Eq. (6) was used in this model. Properties of dry air [16], including the adiabatic index γ and thermal conductivity k_g, were used. An accommodation coefficient of $A = 0.87$ for the Al particle [24] was used. Literature data summarized in [24] indicate that the accommodation coefficient for Al can vary in the range of 0.87–0.97 depending on the surface finish and etching. The value selected in this paper is for a clean, unetched surface that is normally expected to be coated with alumina. Figure 4 shows the Nusselt number as a function of the Knudsen number or particle diameter for a selected combination of particle and gas temperatures. The dashed curve was calculated in [17] for monoatomic gas and was reproduced here. The solid line, used in the present ignition model, shows a modified dependency taking into account properties of air as a diatomic gas.

B. Laser Heating Term

To determine the energy delivered to a particle from the laser beam, consider a particle that crosses a horizontal beam while moving along the vertical axis z. The laser energy delivered to the particle is a function of the particle absorption efficiency η and laser spatial power density $I(z)$, and can be calculated as

$$\dot{Q}_{\text{Laser}} = \tfrac{1}{4}\pi D^2 \eta(\lambda, D, f) I(z) \tag{7}$$

where η is the particle's laser absorption efficiency [21,22] depending on the laser wavelength λ, particle diameter D, and material's complex refractive index f. The laser power density $I(z)$ is commonly described by a Gaussian profile [15] and can be expressed as

$$I(z) = \frac{W}{2\pi\sigma^2}\exp(-z^2/2\sigma^2) \tag{8}$$

where W is the total beam power and σ is the standard deviation for the beam's Gaussian function centered around $z = 0$. The value of σ

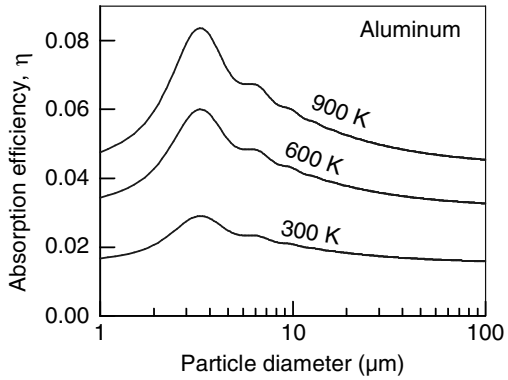

Fig. 5 CO_2 laser beam absorption efficiency as a function of aluminum particle size for different temperatures. The results are obtained in this work and reproduce the data reported earlier [21]. The peak efficiency occurs for the metallic particle diameter of 3.37 μm, nearly independently of material.

(or 6σ approximately equal to the beam diameter D_{beam}) was varied as the model's adjustable parameter, as further discussed.

The laser energy absorption efficiency as a function of particle size and temperature has been described in the literature for spherical metal particles [21,22]. The absorption efficiency was calculated for the temperatures below the particle's melting point using Mie's scattering theory. Drude's model was used to find the complex refractive index as a function of temperature. The computations presented in [21] were reproduced here for aluminum particles, as shown in Fig. 5. The calculations were also performed for other metals and it was observed that for a specific laser wavelength (10.6 μm for the CO_2 laser), the absorption efficiency calculated using Mie's scattering theory [21,22] peaks at nearly the same particle size ($D \approx 3.37$ μm) for different metals. Because of this particle size selective heating, only the particles with the peak absorption efficiency ignite at the threshold laser power in the present experiments. In practical terms, estimates showed that the experimental error in the laser power will lead to ignition of particles within a size range of about 3.3–5 μm.

The model was further modified to account for the effect of melting on the absorption efficiency [23]. On melting, the particle density changes abruptly [16] and the absorption efficiency experiences a jump as shown in Fig. 6. The overall absorption efficiency for a particle undergoing melting was calculated as a weighted average of the efficiencies for its solid and liquid parts.

C. Chemical Term

For Al powder used in the experiments, the ignition model described recently [9–12] was used. The model calculates the rate of oxidation that is limited by the rate of transport of oxygen or aluminum through the protective surface oxide layer. It has been reported that aluminum powders are coated with a 2.5-nm thick layer of amorphous alumina [25–28] which was the assumed initial oxide coating in the model. As the particle temperature increases, different polymorphs of Al_2O_3 become stable [9,29] and the model considers the kinetics of respective polymorphic phase transitions. The transformations accompanied by a significant increase in the density of alumina, such as amorphous to γ alumina and γ to α alumina, can also be accompanied by disruptions in continuity of the protective oxide. Thus, the oxidation rates and respective heat release rates are predicted to increase rapidly when such phase changes occur. Further details of the oxidation model for aluminum particles are available in [12]. The model was validated for aluminum ignition in air [9–12]. Therefore, it is acceptable for a description of the present experiments in which aluminum ignition in air is being considered.

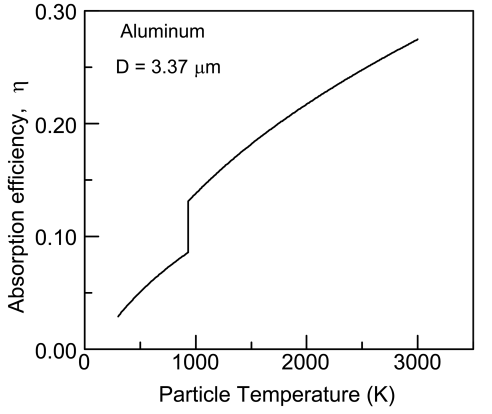

Fig. 6 CO_2 laser beam absorption efficiency as a function of aluminum particle temperature. The jump occurring upon melting is described in [23].

V. Results and Discussion

The model was used to predict the temperature history for a particle crossing a laser beam. The calculations were performed for different particle velocities, corresponding to the experimental aerosol jet velocities. For each calculation, the laser power was allowed to vary to find the threshold power at which ignition was predicted to occur. Figure 7 shows calculated Al particle temperature histories at three different particle velocities. The dashed curves show the particle temperatures when the laser power is just under the ignition threshold. The heating up and cooling down parts of the curves correspond to the particle's entrance to and exit from the laser beam. The solid curves, showing the particle temperature histories at the threshold power, are closely following the dashed curves during the initial heating period. The curves diverge as the particle temperature increases and the role of term $\dot{Q}_{\text{Chemical}}$ becomes increasingly significant.

The calculations were performed until the particle temperature reached the alumina melting point of 2320 K. Above this temperature, the analysis of the heterogeneous processes rate limited by diffusion through the oxide layer is no longer relevant.

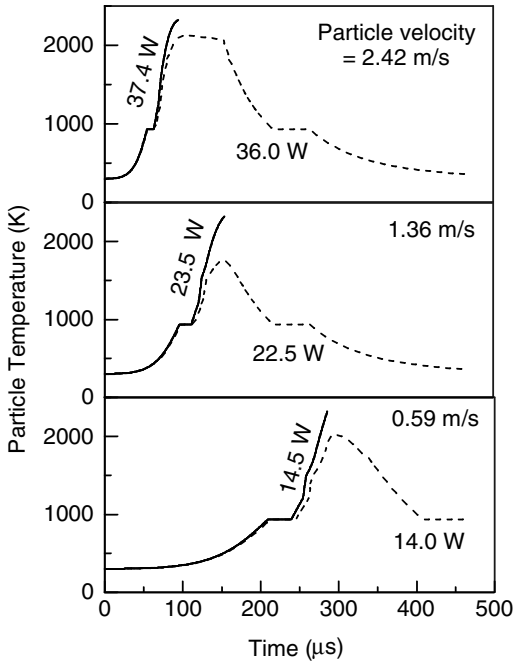

Fig. 7 Temperature histories for laser-heated 3.37-μm diam Al particles calculated for three different particle velocities. The dashed lines show the cases when the laser power is just below the ignition threshold and the solid lines show the cases with the laser power at the threshold.

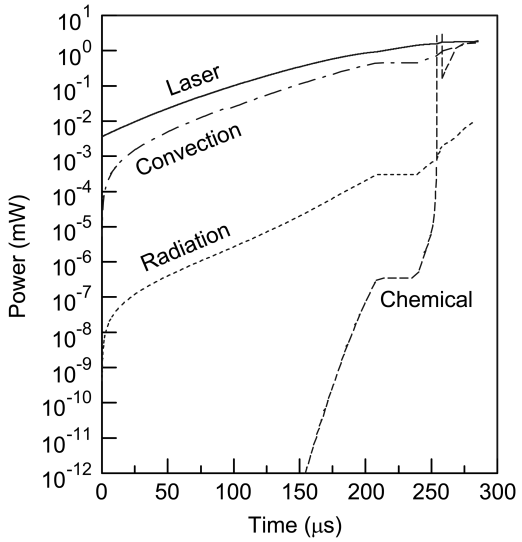

Fig. 8 Different terms of the energy equation (1) for an Al particle of 3.37-μm diameter crossing a CO_2 laser beam, set at 14.5 W at 0.59 m/s.

Furthermore, the oxide coating can no longer remain protective and so the particles that reached this temperature were considered ignited.

Three cases illustrated in Fig. 7 correspond to different heating rates (or different velocities at which the particles crossed the laser beam.) It is clear that at lower heating rates, the predicted ignition threshold laser power is also lower.

A comparison between different terms in the energy equation (1) is shown in Fig. 8 for a case of a particle crossing the laser beam at 0.59 m/s and the laser power set at 14.5 W. Radiation heat losses are insignificant and are always less than 1% of the laser heat input. Therefore, the specific choice of particle emissivity, which is poorly known for the oxidized Al surface, is not important. Convection heat losses represent the dominant heat removal mechanism for the particle. The chemical heat input comes into play and becomes noticeable only after the particle reaches a certain temperature. A sharp increase in the chemical heat generation after the melting plateau is due to a very rapid reaction controlled by the gas phase diffusion to the portion of Al surface exposed to air after the phase transformation from amorphous to γ alumina polymorph [9–12]. Once the openings in the newly formed γ oxide heal, the reaction starts to be controlled by the condensed phase diffusion and a sudden decrease in the rate of chemical heat generation is observed [9,10].

Experimental laser power thresholds for ignition of Al powder at three different particle velocities are shown in Fig. 9. The powder ignited at 14.5, 23.5, and 37.4 W for the particle velocities of 0.59, 1.37, and 2.42 m/s, respectively. For each preset laser power level, the ignition was detected optically, using the PMT ignition peaks. At the threshold power, at least one particle was observed to ignite during a period of 8 s. These ignition statistics are reasonable considering a small number of particles with diameters in the range of 3.3–5 μm among polydispersed aluminum particles fed into the aerosol jet. In addition, only a fraction of particles in the jet crossed the laser beam close to its centerline while the particles crossing the beam at its periphery were heated to a much lower temperature. The error bars for the threshold laser power show the step size used to adjust the laser power experimentally as well as the experimental error in the laser power setting. The error bars shown for the particle velocities represent the standard deviation for the velocity measurements based on the multiple recorded particle streaks.

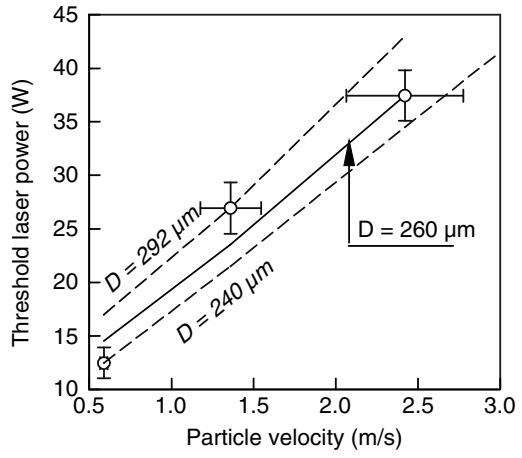

Fig. 9 Experimental results and calculated laser power thresholds for ignition of Al particles for different particle velocities (at different heating rates). Each line is calculated by selecting $6\sigma \approx D_{\text{beam}}$ to match one of the experimental points.

The adjustable parameter 6σ, describing the width of the Gaussian profile for the energy distribution across the laser beam, was varied between 240 and 292 μm to match the experimental laser threshold powers at different heating rates. For each measured threshold laser power corresponding to a specific heating rate, the value of 6σ was found at which the predicted laser power matched the experiment. This value was then used to predict the laser threshold powers for the entire range of heating rates used in experiments. Thus, the three resulting calculated lines are shown in Fig. 9; each line, as described previously, was selected to match one of the experimental points exactly. Most importantly, for all three cases, the overall predicted dependencies of the laser threshold power on the heating rate (or particle velocity) match well with the experimental trend. The value of $6\sigma = 260$ μm, selected for the laser threshold power at the highest heating rate, appears to best match the experimental points at different heating rates and is considered as the final selection for the model's adjustable parameter.

The developed model describes the experiment adequately, and the calibrated heat transfer term describing the CO_2 laser heating of metallic particles can now be used to determine the unknown ignition kinetics for powders other than spherical aluminum used in these experiments. The unknown term $\dot{Q}_{\text{Chemical}}$ can be found by matching the experimental and calculated trends for the laser power ignition threshold as a function of the heating rate and using the terms $\dot{Q}_{\text{Laser}}$, $\dot{Q}_{\text{Radiation}}$, and $\dot{Q}_{\text{Convection}}$ determined above.

VI. Conclusions

A new experimental technique and respective heat transfer model, using transition regime heat transfer, have been developed for studying ignition kinetics of metallic powders at high heating rates. An experimental setup, in which aerosol particles are heated in a CO_2 laser beam, was built and tested. The heating rates on the order of 10^6 K/s were achieved, which are close to those occurring in many practical applications of metal-containing energetic materials. Because the experiment uses a CO_2 laser to heat micron-sized metallic particles, which are comparable to the laser beam wavelength, the heating is most efficient for the particles of a specific diameter, close to 3.37 μm. This particle size-selective heating simplifies dramatically the theoretical analysis of the heat transfer while allowing one to use regular polydispersed powders in experiments. The developed heat transfer model includes radiation, convection in the transition regime, and a detailed analysis of the heat transfer from a laser beam to metal particles. The model was calibrated comparing the calculations and experimental data acquired for spherical Al particles, for which the ignition kinetics parameters were determined elsewhere. The developed experimental technique and the heat transfer model enable one to quantify the kinetics of ignition of a metallic particle in a gaseous environment of interest. The heat transfer term describing the unknown ignition kinetics can be determined by matching the experimental and predicted laser power thresholds necessary for particle ignition at different velocities at which the particles cross the laser beam and, therefore, for different heating rates.

Acknowledgments

This work was supported in part by the Office of Naval Research and the Defense Threat Reduction Agency.

References

[1] Evans, J. P., Borland, W., and Mardon, P. G., "Pyrophoricity of Fine Metal Powders," *Powder Metallurgy*, Vol. 19, No. 1, 1976, pp. 17–21.

[2] Dugam, A. G., Muttalib, A., Gandhi, H. J., Phawade, P. A., John, A., and Khare, R. R., "Effect of Fuel Content and Particle Size Distribution of Oxidizer on Ignition of Metal-Based Pyrotechnic Compositions," *Defence Science Journal*, Vol. 49, No. 3, 1999, pp. 263–268.

[3] Rogers, R. N., "Thermochemistry of Explosives," *Thermochimica Acta*, Vol. 11, No. 2, 1975, pp. 131–139. doi:10.1016/0040-6031(75)80016-5

[4] Pickard, J. M., "Critical Ignition Temperature," *Thermochimica Acta*, Vols. 392–393, Sept. 2002, pp. 37–40. doi:10.1016/S0040-6031(02)00068-0

[5] Annamalai, K., and Durbetaki, P., "A Theory on Transition of Ignition Phase of Coal Particles," *Combustion and Flame*, Vol. 29, No. 2, 1977, pp. 193–208. doi:10.1016/0010-2180(77)90107-9

[6] Almada, S., Campos, J., and Gois, J. C., "Ignition and Pyrolysis of Explosive Components," *Proceedings of the 24th International Pyrotechnics Seminar*, IIT Research Institute, Chicago, 1998, pp. 827–831.

[7] Ward, T. S., Trunov, M. A., Schoentiz, M., and Dreizin, E. L., "Experimental Methodology and Heat Transfer Model for Identification of Ignition Kinetics of Powdered Fuels," *International Journal of Heat and Mass Transfer*, Vol. 49, Nos. 25–26, 2006, pp. 4943–4954. doi:10.1016/j.ijheatmasstransfer.2006.05.025

[8] Shoshin, Y. L., Trunov, M. A., Zhu, X., Schoenitz, M., and Dreizin, E. L., "Ignition of Aluminum-Rich Al–Ti Mechanical Alloys in Air," *Combustion and Flame*, Vol. 144, No. 4, 2006, pp. 688–697. doi:10.1016/j.combustflame.2005.08.037

[9] Trunov, M. A., Schoenitz, M., and Dreizin, E. L., "Ignition of Aluminum Powders Under Different Experimental Conditions," *Propellants, Explosives, Pyrotechnics*, Vol. 30, No. 1, 2005, pp. 36–43. doi:10.1002/prep.200400083

[10] Trunov, M. A., Schoenitz, M., Zhu, X., and Dreizin, E. L., "Effect of Polymorphic Phase Transformations in Al_2O_3 Film on Oxidation Kinetics of Aluminum Powders," *Combustion and Flame*, Vol. 140, No. 4, 2005, pp. 310–318. doi:10.1016/j.combustflame.2004.10.010

[11] Trunov, M. A., Umbrajkar, S. M., Schoenitz, M., Mang, J. T., and Dreizin, E. L., "Oxidation and Melting of Aluminum Nanopowders," *Journal of Physical Chemistry B*, Vol. 110, No. 26, 2006, pp. 13094–13099. doi:10.1021/jp0614188

[12] Trunov, M. A., Schoenitz, M., and Dreizin, E. L., "Effect of Polymorphic Phase Transformations in Alumina Layer on Ignition of Aluminum Particles," *Combustion Theory and Modeling*, Vol. 10, No. 4, 2006, pp. 603–624. doi:10.1080/13647830600578506

[13] Shoshin, Y., and Dreizin, E., "Production of Well-Controlled Laminar Aerosol Jets and Their Application for Studying Aerosol Combustion Processes," *Aerosol Science and Technology*, Vol. 36, No. 9, 2002, pp. 953–962. doi:10.1080/02786820290092131

[14] Shoshin, Y. L., and Dreizin, E. L., "Laminar Lifted Flame Speed Measurements for Aerosols of Metals and Mechanical Alloys," *AIAA Journal*, Vol. 42, No. 7, 2004, pp. 1416–1426.

[15] Yilbas, B. S., "Laser Heating Process and Experimental Validation," *International Journal of Heat and Mass Transfer*, Vol. 40, No. 5, 1997, pp. 1131–1143. doi:10.1016/0017-9310(96)00124-X

[16] Weast, R. C. (ed.), *CRC Handbook of Chemistry and Physics*, 58th ed., CRC Press, Cleveland, OH, 1977.

[17] FIlipov, A. V., and Rosner, D. E., "Energy Transfer Between an Aerosol Particle and Gas at High Temperature Ratios in the Knudsen Transition Regime," *International Journal of Heat and Mass Transfer*, Vol. 43, No. 1, 2000, pp. 127–138. doi:10.1016/S0017-9310(99)00113-1

[18] Lin, F., Dann, K. J., Snelling, D. R., and Smallwood, G. J., "Heat Conduction from a Spherical Nano-Particle: Status of Modeling Heat Conduction in Laser-Induced Incandescence," *Applied Physics B (Lasers and Optics)*, Vol. 83, No. 3, 2006, pp. 355–382. doi:10.1007/s00340-006-2194-1

[19] Fuchs, N. A., "On the Stationary Charge Distribution on Aerosol Particles in a Bipolar Ionic Atmosphere," *Geofisica Pura e Applicata*, Vol. 56, No. 1, 1963, pp. 185–193.

[20] Fuchs, N. A., *The Mechanics of Aerosols*, Macmillan, New York, 1964.

[21] Qiu, T. Q., Longtin, J. P., and Tien, C. L., "Characteristics of Radiation Absorption in Metallic Particles," *Journal of Heat Transfer*, Vol. 117, No. 2, 1995, pp. 340–345.

[22] Bhormen, C. F., and Huffman, D. R., *Absorption and Scattering of Light by Small Particles*, Wiley, New York, 1983, pp. 126–129, Chap. 4.

[23] Graham, S. A., "Absorptivity of Several Metals at 10.6 μm: Empirical Expressions for the Temperature Dependence Computed from Drude Theory," *Applied Optics*, Vol. 23, No. 9, 1984, pp. 1434–1436.

[24] Saxena, S. C., and Joshi, R. K., *Thermal Accommodation and Adsorption Coefficients of Gases*, Hemisphere, New York, 1989.

[25] Doherty, P. E., and Davis R. S., "Direct Observation of the Oxidation of Aluminum Single—Cristal Surfaces," *Journal of Applied Physics*, Vol. 34, No. 3, 1963, pp. 619–628. doi:10.1063/1.1729318

[26] Thomas, K., and Roberts, M. W., " Direct Observation in the Electron Microscope of Oxide Layers of Aluminum," *Journal of Applied Physics*, Vol. 32, No. 1, 1961, pp. 70–75. doi:10.1063/1.1735963

[27] Steinheil, A., "The Structure and Growth of Thin Surface Films on Metals on Oxidation in Air," *Annalen der Physik*, Vol. 19, No. 5, 1934, pp. 465–483.

[28] Ramaswamy, A. L., Kaste, P., and Trevino, S. F., "A Micro-Version of the Physio-Chemical Phenomena Occuring in Nano-Particles of Aluminum," *Journal of Energetic Materials*, Vol. 22, No. 1, 2004, pp. 1–24. doi:10.1080/07370650490438266

[29] Levin, I., and Brandon, D., "Metastable Alumina Polymorphs: Crystal Structures and Transitions Sequences," *Journal of the American Ceramic Society*, Vol. 81, No. 8, 1998, pp. 1995–2012.

S. Son
Associate Editor